Higher flow harmonics from (3+1)D event-by-event viscous hydrodynamics

Björn Schenke, Sangyong Jeon, and Charles Gale

Higher flow harmonics from (3+1)D event-by-event viscous hydrodynamics

Björn Schenke

Physics Department, Brookhaven National Laboratory, Upton, NY-11973, USA

Sangyong Jeon and Charles Gale

Department of Physics, McGill University, 3600 University Street, Montreal, Quebec, H3A 2T8, Canada

We present event-by-event viscous hydrodynamic calculations of the anisotropic flow coefficients v_2 to v_5 for heavy-ion collisions at the Relativistic Heavy-Ion Collider (RHIC). We study the dependence of different flow harmonics on shear viscosity and the morphology of the initial state. v_3 and higher flow harmonics exhibit a particularly strong dependence on both the initial granularity and shear viscosity. We argue that a combined analysis of all available flow harmonics has the potential to determine η/s of the quark gluon plasma more precisely than previously. Presented results strongly hint at a value $(\eta/s)_{QGP} < 2/4\pi$ at RHIC. Furthermore, we demonstrate the effect of shear viscosity on pseudo-rapidity spectra and the mean transverse momentum as a function of rapidity.

I. INTRODUCTION

Hydrodynamics is an indispensable and accurate tool for the description of the bulk behavior of a fluid. The equations of hydrodynamics are just the conservation laws, an additional equation of state and constitutive relationships for dissipative hydrodynamics. The idea that ideal hydrodynamics can describe the outcome of hadronic collisions has a long history. Applications to relativistic heavy-ion collisions have been carried out by many researchers (see [1, 2] for an extensive list of references).

Fluctuating initial conditions for hydrodynamic simulations of heavy-ion collisions have been argued to be very important for the exact determination of collective flow observables and to describe features of multi-particle correlation measurements in heavy-ion collisions [3–22]. Real event-by-event hydrodynamic simulations have been performed and show modifications to spectra and flow from "single-shot" hydrodynamics with averaged initial conditions [17, 20–22]. An important advantage of event-by-event hydrodynamic calculations is the possibility to consistently study all higher flow harmonics in the same simulation. The initial state does not have to be constructed as a smooth distribution with a given eccentricity, triangularity, etc., which will cause simulations to miss some of the dynamics relevant for the calculation of higher flow harmonics. This is particularly important for the computation of v_4, which receives strong contributions from elliptical deformations of the initial state, and v_5, which couples to triangularity from fluctuations and to the ellipticity of the collision geometry [22]. Recent hydrodynamic simulations have highlighted the role of viscous corrections [23], fluctuating initial states [24] and the combination of both [25] also on electromagnetic observables.

Different v_n depend differently on η/s and the details of the initial condition, which is determined by the dynamics and fluctuations of partons in the incoming nuclear wave functions. In this work we present quantitative results on the dependence of v_2 to v_5 on both the shear viscosity to entropy density ratio η/s and the granularity of the initial state, and compare to experimental data.

This paper is organized as follows. In Section II we introduce the employed second order relativistic viscous hydrodynamic framework. The explicit form of the hyperbolic equations in τ-η_s coordinates and the numerical implementation are presented in Section III. We discuss the initial condition for single events in Section IV and explain the freeze-out procedure in Section V. Finally, results are presented in Section VI, followed by conclusions and discussions in Section VII.

II. VISCOUS HYDRODYNAMICS

In [1] we introduced the simulation MUSIC for ideal relativistic fluids and extended it in [20] to include dissipative effects.

In the ideal case, the evolution of the system, created in relativistic heavy-ion collisions, is described by the following 5 conservation equations

$$\partial_\mu T_0^{\mu\nu} = 0 , \tag{1}$$
$$\partial_\mu J_B^\mu = 0 , \tag{2}$$

where $T_0^{\mu\nu}$ is the energy-momentum tensor and J_B^μ is the net baryon current. These are usually re-expressed using the time-like flow 4-vector u^μ as

$$T_0^{\mu\nu} = (\varepsilon + \mathcal{P})u^\mu u^\nu - \mathcal{P}g^{\mu\nu} , \tag{3}$$
$$J_B^\mu = \rho_B u^\mu , \tag{4}$$

where ε is the energy density, $\mathcal{P}$ is the pressure, ρ_B is the baryon density and $g^{\mu\nu} = \mathrm{diag}(1, -1, -1, -1)$ is the metric tensor. The equations are then closed by adding the equilibrium equation of state

$$\mathcal{P} = \mathcal{P}(\varepsilon, \rho_B) \tag{5}$$

as a local constraint on the variables.

Historically, these equations have first been solved in a boost-invariant framework [26], eliminating the longitudinal direction and assuming uniformity in the trans-

verse direction. At RHIC the central plateau in rapidity extends over 4 units. Hence, as long as one is concerned only with the dynamics near the mid-rapidity region, boost invariance should be a valid approximation at RHIC, restricting the relevant spatial dimensions to the transverse plane. Much success has been achieved by these (2+1)D calculations (see references in [1] and [27, 28] for thorough reviews). However, in order to analyze experimental data away from mid-rapidity, inclusion of the non-trivial longitudinal dynamics is essential [1, 29–34].

The next step in improving relativistic hydrodynamic simulations of heavy-ion collisions is the inclusion of finite viscosities. In the first order, or Navier-Stokes formalism for viscous hydrodynamics, the stress-energy tensor is decomposed into

$$T_{1st}^{\mu\nu} = T_0^{\mu\nu} + S^{\mu\nu} \,, \tag{6}$$

where $T_0^{\mu\nu}$ is given by Eq. (3)

The viscous part of the stress energy tensor in the first-order approach is given by

$$S^{\mu\nu} = \eta \left(\nabla^\mu u^\nu + \nabla^\nu u^\mu - \frac{2}{3} \Delta^{\mu\nu} \nabla_\alpha u^\alpha \right) \tag{7}$$

where $\Delta^{\mu\nu} = g^{\mu\nu} - u^\mu u^\nu$ is the local 3-metric and $\nabla^\mu = \Delta^{\mu\nu} \partial_\nu$ is the local spatial derivative. Note that $S^{\mu\nu}$ is transverse with respect to the flow velocity since $\Delta^{\mu\nu} u_\nu = 0$ and $u^\nu u_\nu = 1$. Hence, u^μ is also an eigenvector of the whole stress-energy tensor with the same eigenvalue ϵ. η is the shear viscosity of the medium. We assume the ratio η/s to be constant. This way we can study the dependence of observables on an effective η/s, neglecting its temperature dependence that has been studied in e.g. [35, 36]. In particular, we do not take into account an increasing η/s in the hadronic phase which should preferably be done by switching to a hadronic rescattering simulation when viscous corrections become large. Not aiming at a precision determination of $\eta/s(T)$ in the current work these approximations are adequate.

The form of viscous hydrodynamics using (7) is conceptually simple. However, this Navier-Stokes form is known to introduce unphysical super-luminal signals [37–39], leading to numerical instabilities. The second-order Israel-Stewart formalism [40–42] avoids this super-luminal propagation, as does the more recent approach in [43].

In this work, we use a variant of the Israel-Stewart formalism derived in [44], where the stress-energy tensor is decomposed as

$$T^{\mu\nu} = T_0^{\mu\nu} + \pi^{\mu\nu} \,. \tag{8}$$

The evolution equations are

$$\partial_\mu T^{\mu\nu} = 0 \tag{9}$$

and

$$\Delta_\alpha^\mu \Delta_\beta^\nu u^\sigma \partial_\sigma \pi^{\alpha\beta} = -\frac{1}{\tau_\pi} \left(\pi^{\mu\nu} - S^{\mu\nu} \right) - \frac{4}{3} \pi^{\mu\nu} (\partial_\alpha u^\alpha) \,. \tag{10}$$

When dealing with rapid longitudinal expansion, it is useful to transform these equations to the τ-η_s-coordinate system, defined by

$$t = \tau \cosh \eta_s \,,$$
$$z = \tau \sinh \eta_s \,. \tag{11}$$

We obtain the following hyperbolic equations with sources

$$\partial_a T_0^{ab} = -\partial_a \pi^{ab} + F^b \tag{12}$$

and

$$\partial_a (u^a \pi^{cd}) = -(1/\tau_\pi)(\pi^{cd} - S^{cd}) + G^{cd} \tag{13}$$

where F^b and G^{cd} contain terms introduced by the coordinate change from t, z to τ, η_s as well as those introduced by the projections in Eq. (10), and τ_π is the relaxation time. Latin indeces a, b, c, d indicate that we are in the τ-η_s-coordinate system. Summation over all four dimensions is implied for repeated indeces.

Our approach to solve these hyperbolic equations relies on the Kurganov-Tadmor (KT) scheme [45, 46], together with Heun's method to solve resulting ordinary differential equations.

III. IMPLEMENTATION

As mentioned above, the most natural coordinate system for us is the $\tau - \eta_s$ coordinate system defined by Eq. (11). In this coordinate system, the conservation equation $\partial_\mu J^\mu = 0$ becomes

$$\partial_\tau (\tau J^\tau) + \partial_v (\tau J^v) + \partial_{\eta_s} J^{\eta_s} = 0 \,, \tag{14}$$

where

$$J^\tau = (\cosh \eta_s J^0 - \sinh \eta_s J^3) \,, \tag{15}$$
$$J^{\eta_s} = (\cosh \eta_s J^3 - \sinh \eta_s J^0) \,, \tag{16}$$

which is simply a Lorentz boost with the space-time rapidity $\eta_s = \tanh^{-1}(z/t)$. The index v and w in this section always refer to the transverse x, y coordinates which are not affected by the boost. Repeated indices v or w imply summation over x and y only. Applying the same transformation to both indices in Eq. (9), one obtains

$$\partial_\tau (\tau T_0^{\tau\tau}) + \partial_v (\tau T_0^{v\tau}) + \partial_{\eta_s} (T_0^{\eta_s\tau}) + T_0^{\eta_s\eta_s} \tag{17}$$
$$+ \partial_\tau (\tau \pi^{\tau\tau}) + \partial_v (\tau \pi^{v\tau}) + \partial_{\eta_s} (\pi^{\eta_s\tau}) + \pi^{\eta_s\eta_s} = 0 \,,$$

$$\partial_\tau (\tau T_0^{\tau\eta_s}) + \partial_v (\tau T_0^{v\eta_s}) + \partial_{\eta_s} (T_0^{\eta_s\eta_s}) + T_0^{\tau\eta_s} \tag{18}$$
$$+ \partial_\tau (\tau \pi^{\tau\eta_s}) + \partial_v (\tau \pi^{v\eta_s}) + \partial_{\eta_s} (\pi^{\eta_s\eta_s}) + \pi^{\tau\eta_s} = 0 \,,$$

and

$$\partial_\tau (\tau T_0^{\tau v}) + \partial_w (\tau T_0^{wv}) + \partial_{\eta_s} (T_0^{\eta_s v}) \tag{19}$$
$$+ \partial_\tau (\tau \pi^{\tau v}) + \partial_w (\tau \pi^{wv}) + \partial_{\eta_s} (\pi^{\eta_s v}) = 0 \,.$$

These 5 equations, namely Eq. (14) for the net baryon current, and Eqs. (17, 18, 19) for the energy and momentum, are solved along with Eqs. (13) for the viscous part of the stress-energy tensor, which in a more explicit way of writing read

$$
\begin{aligned}
\partial_c(u^c\pi^{ab}) = & -\frac{1}{2\tau}u^\tau\pi^{ab} + \frac{1}{\tau}\Delta^{a\eta}u^\eta\pi^{b\tau} - \frac{1}{\tau}\Delta^{a\tau}u^\eta\pi^{b\eta} \\
& - g_{cf}\pi^{cb}u^a Du^f - \frac{\pi^{ab}}{2\tau_\pi} - \frac{1}{6}\pi^{ab}\partial_c u^c \\
& + \frac{\eta}{\tau_\pi}\left(-\frac{1}{\tau}\Delta^{a\eta}g^{b\eta}u^\tau + \frac{1}{\tau}\Delta^{a\eta}g^{b\tau}u^\tau \right. \\
& \left. + g^{ac}\partial_c u^b - u^a Du^b - \frac{1}{3}\Delta^{ab}\partial_c u^c\right) \\
& + (a \leftrightarrow b),
\end{aligned}
\tag{20}
$$

The relaxation time τ_π is set to $3\eta/(\epsilon + \mathcal{P})$, in line with the approach in [47]. It was also shown in [48] that the dependence of observables such as v_2 on τ_π is negligible when including the term $(4/3)\pi^{\mu\nu}(\partial_\alpha u^\alpha)$ in Eq. (10).

To solve the equations we use the KT algorithm as explained in [1]. In detail, we compute the first step within Heun's method for Eqs. (14, 17, 18, 19), then the first step for Eqs. (20), proceed with the second step for Eqs. (14, 17, 18, 19) using the evolved result for π^{ab}, and finally compute the second step for Eqs. (20). This concludes the evolution of one time step.

One major difference to the ideal hydrodynamic equations solved in [1] is the appearance of time derivatives in the source terms of Eqs. (17, 18, 19, 20). These are handled with the first order approximation

$$
\dot{g}(\tau_n) = (g(\tau_n) - g(\tau_{n-1}))/\Delta\tau,
\tag{21}
$$

in the first step of the Heun method, and in the second step we use

$$
\dot{g}(\tau_n) = (g^*(\tau_{n+1}) - g(\tau_n))/\Delta\tau,
\tag{22}
$$

where $g^*(\tau_{n+1})$ is the result from the first step.

As in most Eulerian algorithms, ours also suffers from numerical instability when the density becomes small while the flow velocity becomes large. Fortunately this happens late in the evolution or at the very edge of the system. Regularizing such instability has no strong effects on the observables we are interested in. Some ways of handling this are known (for instance see Ref. [49]).

In this study, when finite viscosity causes negative pressure in the cell, we revert to the previous value of $\pi^{\mu\nu}$ and reduce all components by 5%. This procedure stabilizes the calculations without introducing spurious effects.

IV. INITIALIZATION AND EQUATION OF STATE

To determine the energy density distribution at the initial time τ_0 for a single event, we employ the Monte-Carlo Glauber model using the method described in [50] to determine the initial distribution of wounded nucleons. Before the collision the density distribution of the two nuclei is described by a Woods-Saxon parametrization, which we sample to determine the positions of individual nucleons. The impact parameter is sampled from the distribution

$$
P(b)db = 2bdb/(b_{\max}^2 - b_{\min}^2),
\tag{23}
$$

where $b_{\min}$ and $b_{\max}$ depend on the given centrality class. Given the sampled initial impact parameter the two nuclei are superimposed. Two nucleons are assumed to collide if their relative transverse distance is less than

$$
D = \sqrt{\sigma_{NN}/\pi},
\tag{24}
$$

where σ_{NN} is the inelastic nucleon-nucleon cross-section, which at top RHIC energy of $\sqrt{s} = 200A$ GeV is $\sigma_{NN} = 42$ mb. The energy density is taken to scale mostly with the wounded nucleon distribution and to 25% with the binary collision distribution. So, two distributions are generated, one where for every wounded nucleon a contribution to the energy density with Gaussian shape and width σ_0 in both x and y is added, one where the same is done for every binary collision. These are then multiplied by 0.75 and 0.25, respectively, and added.

In the rapidity direction, we assume the energy density to be constant on a central plateau and fall like half-Gaussians at large $|\eta_s|$ as described in [1]:

$$
\varepsilon(\eta_s) \propto \exp\left[-\frac{(|\eta_s| - \eta_{\mathrm{flat}}/2)^2}{2\sigma_\eta^2}\theta(|\eta_s| - \eta_{\mathrm{flat}}/2)\right]
\tag{25}
$$

This procedure generates flux-tube like structures compatible with measured long-range rapidity correlations [51–53]. The absolute normalization is determined by demanding that the obtained total multiplicity distribution reproduces the experimental data. We initialize with $\pi^{\mu\nu}(\tau_0) = 0$.

As equation of state we employ the parametrization "s95p-v1" from [54], obtained from interpolating between lattice data and a hadron resonance gas. This equation of state describes a chemically equilibrated system and hence does not account for chemical decoupling before kinetic freeze-out. Equations of state including partial chemical equilibrium improve on this and will be studied in future work.

V. FREEZE-OUT

We perform a Cooper-Frye freeze-out using

$$
E\frac{dN}{d^3p} = \frac{dN}{dyp_Tdp_Td\phi_p} = g_i\int_\Sigma f(u^\mu p_\mu)p^\mu d^3\Sigma_\mu,
\tag{26}
$$

where g_i is the degeneracy of particle species i, and Σ the freeze-out hyper-surface. In the ideal case the distri-

bution function is given by

$$f(u^\mu p_\mu) = f_0(u^\mu p_\mu) = \frac{1}{(2\pi)^3} \frac{1}{\exp((u^\mu p_\mu - \mu_i)/T_{\rm FO}) \pm 1},$$ (27)

where μ_i is the chemical potential for particle species i and $T_{\rm FO}$ is the freeze-out temperature. In the finite viscosity case we include viscous corrections to the distribution function, $f = f_0 + \delta f$, with

$$\delta f = D(\alpha) f_0 (1 \pm (2\pi)^3 f_0) \left(\frac{T}{E}\right)^\alpha p^\mu p^\nu \pi_{\mu\nu} \frac{1}{2(\epsilon + \mathcal{P})T^2},$$ (28)

where π is the viscous correction introduced in Eq. (8). This result is obtained using a relaxation time approximation [55]. $\alpha \in [0, 1]$ depends on the details of the (unknown) underlying microscopic theory, $E = p_\mu u^\mu$, and $D(\alpha) = 120/\Gamma(6 - \alpha)$ is a normalization factor derived using Boltzmann statistics in the kinetic theory (differences to quantum statistics are on the one percent level). $\Gamma(\cdot)$ is the Euler gamma function. Most presented results are obtained using $\alpha = 0$, leading to $\delta f \sim p^2$, but this choice is not unique [55]. Therefore we will show a comparison of all $v_n(p_T)$ using $\alpha = 0, 0.5$ and 1 to see how large an uncertainty is introduced in the final result by the uncertainty in δf.

The algorithm used to determine the freeze-out surface Σ has been presented in [1]. It can be used without modification for determining the freeze-out surface of a system with fluctuating initial conditions. In this case the error introduced by complicated surface shapes where the surface can not be constructed without gaps is less than 1%.

VI. ANALYSIS AND RESULTS

While in standard hydrodynamic simulations with averaged initial conditions all odd flow coefficients vanish by definition, fluctuations generate all flow harmonics as response to the initial geometry. We follow [19], where v_3 is computed in a similar way to the standard event plane analysis for elliptic flow, and for each v_n define an event plane through the angle

$$\psi_n = \frac{1}{n} \arctan \frac{\langle \sin(n\phi) \rangle}{\langle \cos(n\phi) \rangle}.$$ (29)

Note that here we do not weigh the average by p_T as done in [19, 20] and [56]. Definition (29) is closer to what is done in the PHENIX experiment, because the p_T of the particles used to determine the event planes are not measured. Therefore one can not apply an explicit p_T weighting [57]. Most of the particles used to determine the event plane have low transverse momentum because of the fast dropping spectrum. Differences between the different definitions are however small and lead to variations of v_n on the order of one percent or less.

The flow coefficients can be computed using

$$v_n = \langle \cos(n(\phi - \psi_n)) \rangle.$$ (30)

When averaging over events we compute the root mean square $\sqrt{\langle v_2^2 \rangle}$ because we compare to data obtained with the event-plane method (see [58]). First, we present results for particle spectra as functions of p_T and η_s. Parameters were chosen in order to reproduce the experimental data for the spectra when including all resonances up to 2 GeV (and some higher lying resonances to be consistent with what is included in the employed equation of state). The used parameters can be found in Table I. Values for the maximal average energy density (in the center of the system) $\langle \varepsilon_{\max} \rangle$ are quoted for most central (0-5%) collisions. In addition, all parameter sets use $\eta_{\rm flat} = 4.8$ and $\sigma_\eta = 0.7$.

η/s	σ_0[fm]	τ_0[fm/c]	$\langle \varepsilon_{\max} \rangle$[GeV/fm^3]	$T_{\rm FO}$[MeV]
0	0.4	0.4	65.7	150
0.08	0.4	0.4	57	150
0.16	0.4	0.4	50	150
0.08	0.2	0.4	57	155
0.08	0.8	0.4	57	145

TABLE I. Parameter sets.

Fig. 1 shows the transverse momentum spectra of positive pions, kaons and protons compared to experimental data from PHENIX [59] in 20-30% central events. In Fig. 2 we present a comparison of the computed charged particle spectrum for $\eta/s = 0.08$ in 15-25% central collisions as a function of pseudo-rapidity η_p with experimental data from PHOBOS [60].
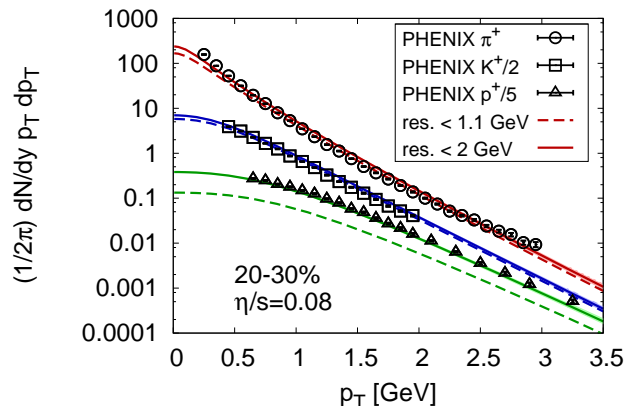

FIG. 1. (Color online) Positive pion transverse momentum spectrum for 20-30% central Au+Au collisions using $\eta/s = 0.08$ including resonances up to 2 GeV (solid) and up to the ϕ-meson (dashed) compared to data from PHENIX [59]. Results are averages over 10 single events.
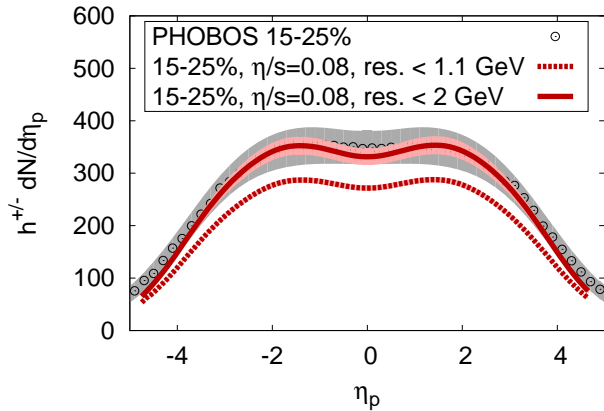
FIG. 2. (Color online) Charged hadron spectrum for 15-25%
central Au+Au collisions including resonances up to $2\,\text{GeV}$
(solid, averaged over 10 events) and up to the ϕ-meson (dot-
ted, averaged over 100 events) compared to data from PHO-
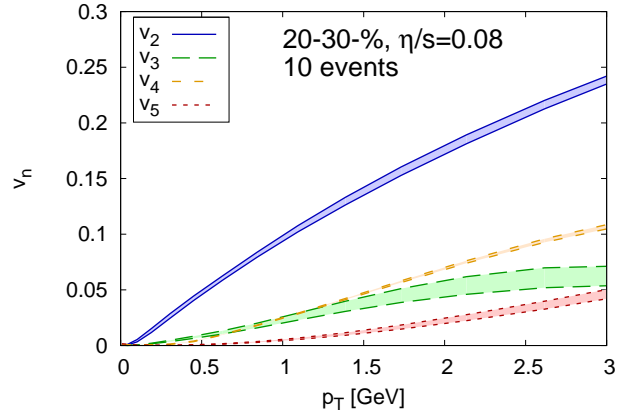BOS [60].

FIG. 3. (Color online) Charged hadron v_2 to v_5 for $\eta/s = 0.08$
as a function of transverse momentum p_T averaged over 10
single events, including resonances up to the ϕ-meson (upper
end of each band) and all resonances up to $2\,\text{GeV}$ (lower end
of each band).

With the employed parameters we achieve very good
agreement when including all resonance decays. In gen-
eral, it is computationally too expensive to include reso-
nances up to $2\,\text{GeV}$ for all calculations. Hence, for most
presented results we restrict ourselves to including reso-
nances up to the ϕ-meson only. This is a good approx-
imation because pions dominate the flow of all charged
hadrons and it is mainly the ρ- and ω- mesons that mod-
ify the pion distributions. Fig. 3 shows how the v_n for
charged hadrons are affected by including different num-
bers of resonances. Including more resonances reduces
all v_n, however, the quantitative effect is small. The re-
duction is caused by the kinematics of resonance decays.
When including more resonances, decays will diffuse the
distribution of lower lying resonances and finally that of
pions, kaons, and protons. This diffusion leads to weaker
anisotropic flow. The influence of higher lying resonances
on v_3 appears to be larger than that on the other v_n.

Next, we verify that our results are not plagued by
large discretization errors. Higher flow harmonics are
sensitive to fine structures in the system and for the case
of ideal hydrodynamics with smooth initial conditions it
was shown in [1] that v_4 is very sensitive to the lattice
spacing if it is not chosen small enough. Fig. 4 shows
$v_n(p_T)$ for two different lattice spacings, our standard
value of $a = 0.115\,\text{fm}$ and a larger $a = 0.2\,\text{fm}$. Differences
are within the statistical error bars from averaging over
100 events each.

In Fig. 5 we demonstrate the uncertainty in all $v_n(p_T)$
introduced by the uncertainty in the viscous correction
δf to the thermal distribution function. Using $\alpha = 0, 0.5$,
and 1 corresponding to $\delta f \propto p^2, p^{3/2}$, and p, respectively,
as well as no δf-correction at all, we find that the un-
certainty from δf for $p_T < 2\,\text{GeV}$ is negligible and still
moderate for $2\,\text{GeV} < p_T < 3\,\text{GeV}$. Our results are hence
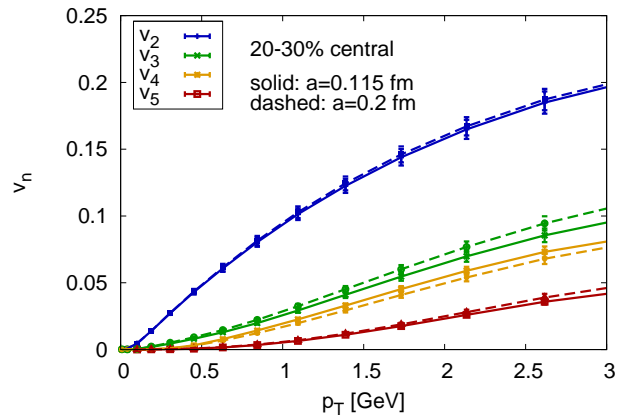
FIG. 4. (Color online) Charged hadron v_2 to v_5 for $\eta/s =
0.08$ and $\sigma_0 = 0.4\,\text{fm}$ as a function of transverse momentum
p_T averaged over 100 single events for lattice spacings $a =
0.115\,\text{fm}$ (solid lines) and $a = 0.2\,\text{fm}$ (dashed lines).

robust for $p_T < 2\,\text{GeV}$.

Because we are using a (3+1)-dimensional relativis-
tic viscous hydrodynamic simulation, it is interesting
to demonstrate the effect of shear viscosity on the lon-
gitudinal dynamics of the system, which in a (1+1)-
dimensional simulation was studied in [61, 62].

Fig. 6 shows the modification of charged hadron
pseudo-rapidity spectra caused by the inclusion of shear
viscosity. The shape of the initial energy density distri-
bution in the longitudinal direction is the same for all
curves, which were each averaged over 200 events. The
normalization was adjusted to yield the same multiplicity
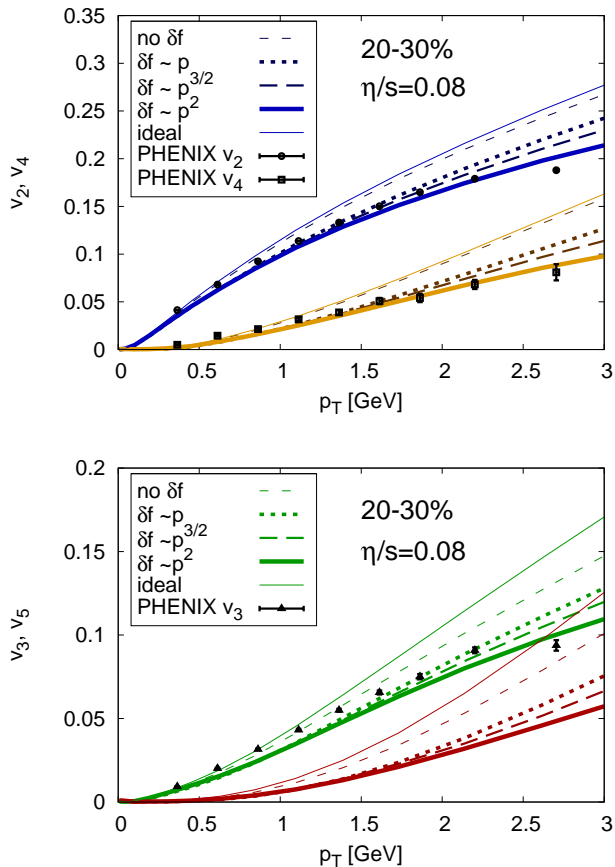at midrapidity in all cases. In the range $2 < |\eta_p| < 4$ the

FIG. 5. (Color online) Differential v_2 and v_4 (upper panel) and v_3 and v_5 (lower panel) in 20-30% central collisions using $\eta/s = 0.08$ and varying the p-dependence of δf. Also shown is the ideal result and the result from viscous evolution only (no δf). We are not showing error bands for clarity. Results are averages over 100 single events each.

to the difference in longitudinal and transverse expansion, entropy production is largest in this region, which we have checked explicitly. The large shear stress in this region subsequently leads to larger transverse pressure, hence larger transverse pressure gradients. This leads to an increased transverse velocity at intermediate rapidities, explaining the increased average p_T. The shear stress remains large until freeze-out leading to the larger δf correction in the same region.
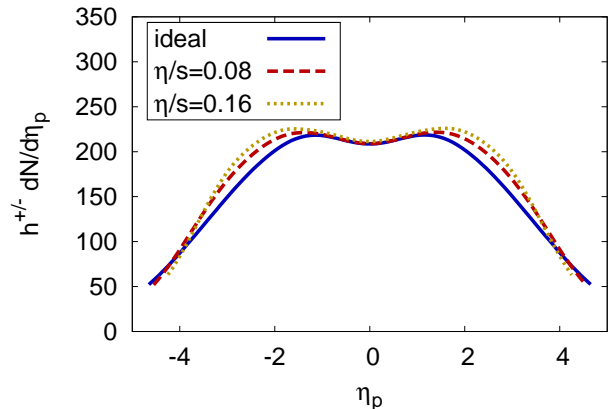

FIG. 6. (Color online) Charged hadron spectrum for 20-30% central Au+Au collisions for different values of η/s including resonances up to the ϕ-meson.

pseudo-rapidity spectra are increased, for larger η_p decreased by the effect of shear viscosity. We checked that this effect is almost entirely due to the modified evolution when including shear viscosity. The viscous correction to the distribution functions δf (28) only causes minor modifications. Additional information can be obtained by looking at the average transverse momentum $\langle p_T \rangle$ as a function of rapidity. We show in Fig. 7 that also $\langle p_T \rangle$ increases at intermediate rapidities and decreases at the largest $|y|$. For this observable the effect of δf is larger.

In the viscous case, the effective longitudinal pressure is reduced compared to an ideal fluid. Hence longitudinal pressure gradients are smaller and longitudinal acceleration is reduced, leading to smaller multiplicity at the largest rapidities. Also, at the largest rapidities the system is small and freezes out early at low transverse velocity, leading to a small $\langle p_T \rangle$. At intermediate rapidities, the strong change in the initial distribution leads to the largest pressure gradients. Hence, longitudinal expansion is strongest in that region. Because shear is proportional
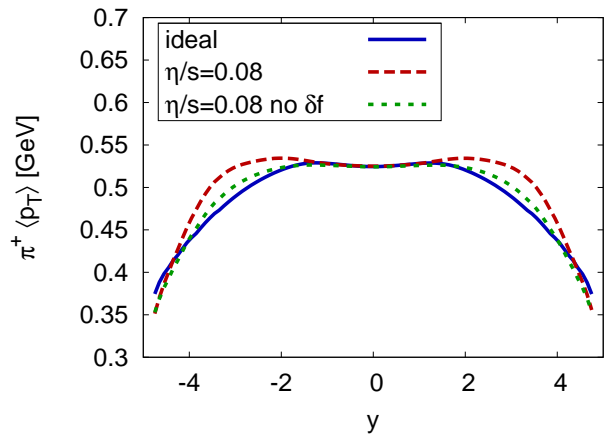

FIG. 7. (Color online) Positive pion average p_T as a function of rapidity y for 20-30% central Au+Au collisions from ideal and viscous ($\eta/s = 0.08$) including resonances up to the ϕ-meson.

In Fig. 8 we show the dependence of $v_n(p_T)$ on the shear viscosity of the system. Results are averaged over 200 single events each. For v_2 to v_4 we compare to experimental data from the PHENIX collaboration obtained using the event plane method [63]. The dependence of $v_n(p_T)$ on η/s increases with increasing n. To make this
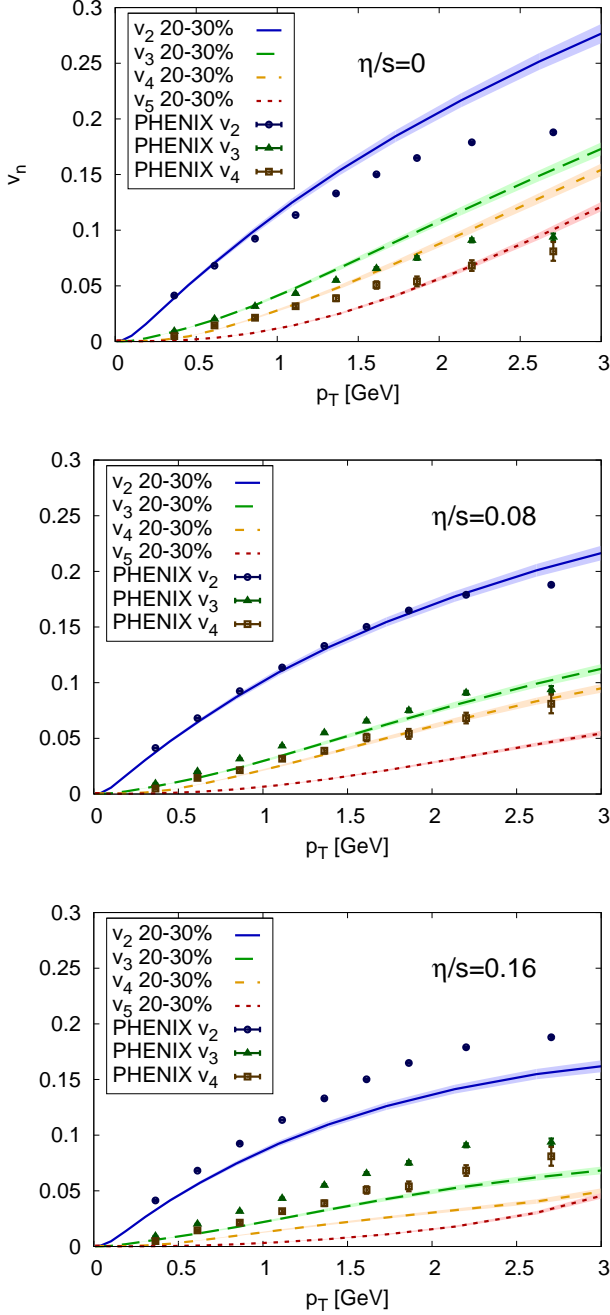
FIG. 8. (Color online) p_T-differential v_2 to v_5 from ideal hydrodynamics (left), viscous hydrodynamics with $\eta/s = 0.08$ (middle), and $\eta/s = 0.16$ (right). Results are averaged over 200 events each. Experimental data from PHENIX [63].

havior is expected because diffusive processes smear out finer structures corresponding to higher n more efficiently than larger scale structures, and has been pointed out previously in [18].

So far all results were obtained using initial conditions with a Gaussian width $\sigma_0 = 0.4$ fm. We now study the effect of the initial state granularity on the flow harmonics by varying σ_0. Decreasing σ_0 causes finer structures to appear and hence strengthens the effect of hot spots. This results in a hardening of the spectra as previously demonstrated in [17]. Because we want to compare to experimental data, we readjust the slopes to match the experimental p_T-spectra by modifying the freeze-out temperature (see Table I).

Fig. 10 shows the dependence of $v_n(p_T)$ on the value of σ_0, which we vary from 0.2 fm to 0.8 fm. While v_2 is almost independent of σ_0, higher flow harmonics show a very strong dependence. In Fig. 11 we present the dependence of the p_T-integrated v_n on the initial state granularity characterized by σ_0.

Higher flow harmonics turn out to be a more sensitive probe of initial state granularity than v_2. While we are not yet attempting an exact extraction of η/s using higher flow harmonics, our results give a first quantitative overview of the effects of both the initial state granularity and η/s on all higher flow harmonics up to v_5. Comparing Figs. 8 and 10, we see that $v_4(p_T)$ obtained from simulations using $\eta/s = 0.16$ is about a factor of 2 below the experimental result, and that decreasing σ_0 by a factor of two does not increase it nearly as much. Note that $\sigma_0 = 0.2$ fm is already a very small value given that we assign this width to a wounded nucleon. It is hence unlikely that a higher initial state granularity will be able to compensate for the large effect of the shear viscosity. Similar arguments hold for $v_3(p_T)$.
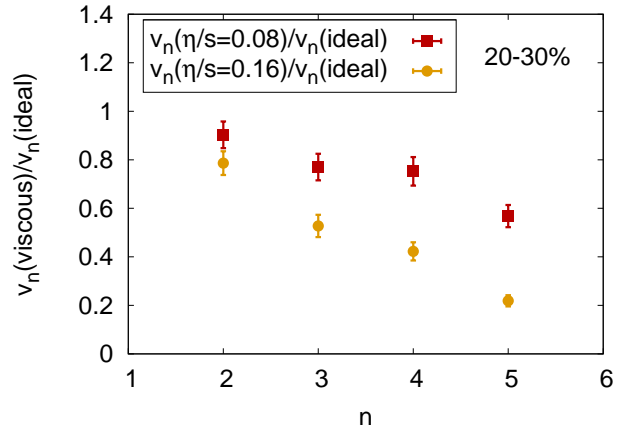

FIG. 9. (Color online) Ratio of charged hadron flow harmonics in viscous simulations to the result from ideal hydrodynamics. Results are averages over 200 single events each.

point more quantitative, we present the ratio of the p_T-integrated v_n from viscous calculations to v_n from ideal calculations as a function of n in Fig. 9. While v_2 is suppressed by $\sim 20\%$ when using $\eta/s = 0.16$, v_5 is suppressed by $\sim 80\%$. Higher harmonics are substantially more affected by the system's shear viscosity than v_2 and hence are a much more sensitive probe of η/s. This be-

A detailed systematic analysis of different models for the initial state with a sophisticated description of fluc-

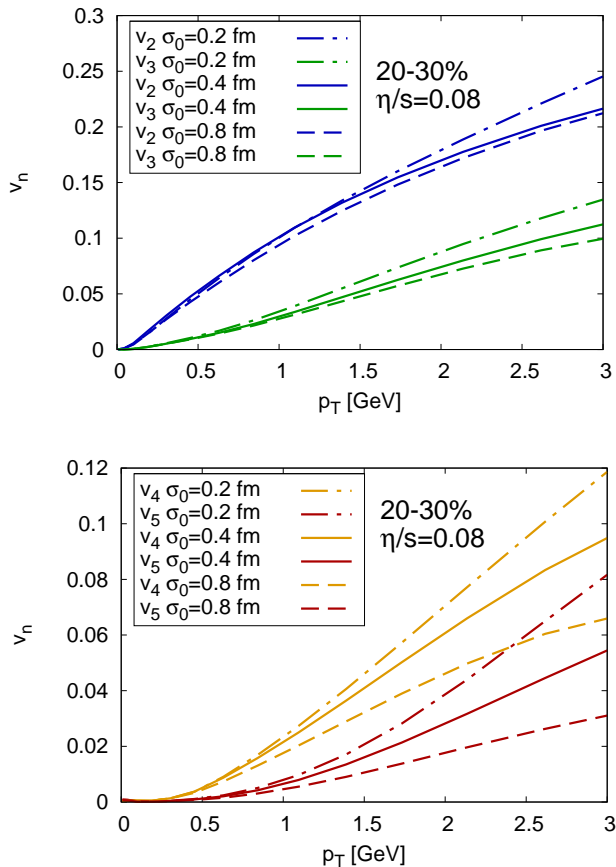collisions indicate that our rather simplistic description of the initial state and its fluctuations is insufficient. Improvements can be made by a systematic study with alternative models for the fluctuating initial state based on e.g. the color-glass-condensate effective theory (along the lines of [66]).

Finally, the higher flow harmonics integrated over a transverse momentum range $0.2\,\text{GeV} < p_T < 2\,\text{GeV}$ are shown in Fig. 14 as a function of centrality. v_2 has the strongest dependence on the centrality because it is driven to a large part by the overall geometry. The odd harmonics are entirely due to fluctuations as we have discussed earlier, and hence do not show a strong dependence on the centrality of the collision.

VII. SUMMARY AND CONCLUSIONS

We have demonstrated that the analysis of higher flow harmonics within (3+1)-dimensional event-by-event viscous hydrodynamics has the potential to determine transport coefficients of the QGP such as η/s much more precisely than the analysis of elliptic flow alone. We presented in detail the framework of (3+1)-dimensional viscous relativistic hydrodynamics and the concept of event-by-event simulations, which enable us to study quantities that are strongly influenced or even entirely due to fluctuations such as odd flow harmonics. Parameters of the hydrodynamic simulation were fixed to reproduce particle spectra both as a function of transverse momentum p_T and pseudo-rapidity η_p. The studied flow harmonics v_2 to v_5 were found to depend increasingly strongly on the value of η/s and also on the initial state granularity. This work does not attempt an exact extraction of η/s of the QGP, and additional work is needed to do so, however, our quantitative results hint at a value of η/s not larger than $2/4\pi$. The reason is the strong suppression of v_3 to v_5 by the shear viscosity. A higher granularity of the initial state counteracts this effect, but our results indicate that this increase is not large enough to account for $\eta/s \geq 2/4\pi$. We will report on a detailed analysis of higher flow harmonics at LHC energies and a comparison to the experimental data in a subsequent work.
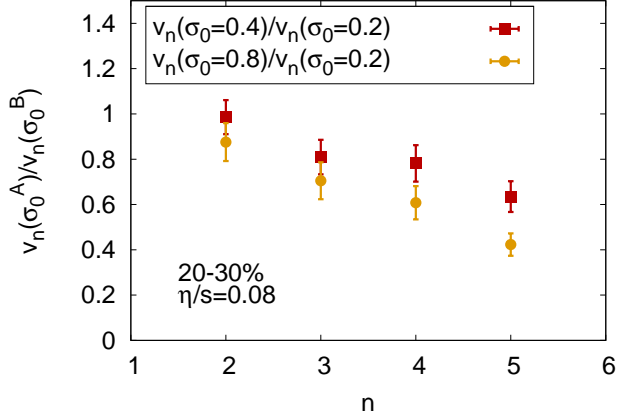

FIG. 10. (Color online) Differential v_2 and v_3 (upper panel) and v_4 and v_5 (lower panel) in 20-30% central collisions using $\eta/s = 0.08$ and varying σ_0. Results are averages over 100 single events each (200 events for $\sigma_0 = 0.4\,\text{fm}$).

tuations is needed to make more precise statements on the value of η/s. Also an equation of state that includes a partial chemical freeze-out is expected to modify the results, in particular $v_n(p_T)$ [64].

It is however clear from the present analysis that the utilization of higher flow harmonics can constrain models for the initial state and values of transport coefficients of the quark-gluon plasma significantly. The analysis of only elliptic flow is not sufficient for this task, because it depends too weakly on both the initial state granularity and η/s.

We present v_2 and v_3 as a function of pseudo-rapidity in Fig. 12. The $v_2(\eta_p)$ result from the simulation is flatter than the experimental data out to $\eta_p \approx 3$ and then falls off more steeply. A modified shape of the initial energy density distribution in the η_s-direction, the inclusion of finite baryon number, and inclusion of a rapidity dependence of the fluctuations will modify the result.

In Fig. 13 we show results of $v_n(p_T)$ for different centralities using $\eta/s = 0.08$. Overall, all flow harmonics are reasonably well reproduced. Deviations from the experimental data, especially of $v_3(p_T)$ in the most central

FIG. 11. (Color online) Ratio of v_n with initial granularity characterized by the Gaussian width $\sigma_0 = 0.8$ fm to the case with $\sigma_0 = 0.4$ fm and $\sigma_0 = 0.8$ fm, respectively. Results are for 20-30% central collisions using $\eta/s = 0.08$. Averages are over 100 single events each.
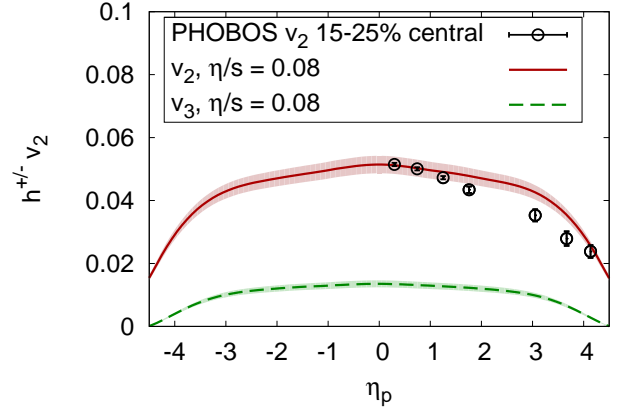

FIG. 12. (Color online) v_2 and v_3 as functions of pseudo-rapidity η_p compared to data from PHOBOS [65]. Averages are over 100 single events each.
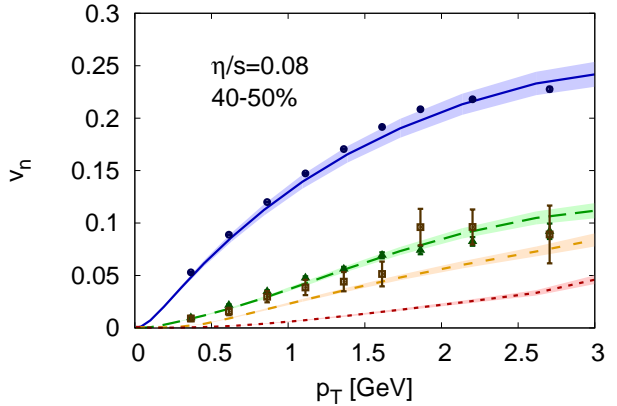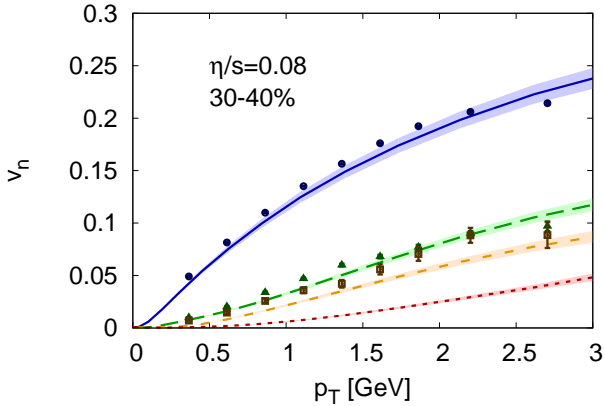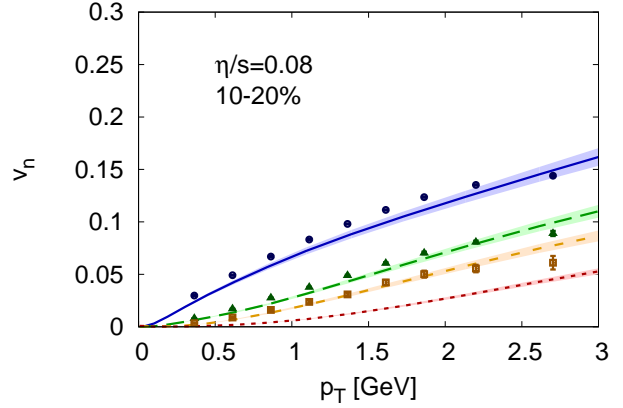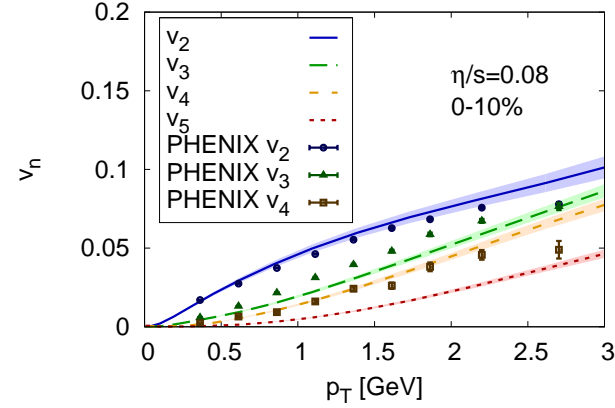

FIG. 13. (Color online) p_T-differential v_2 to v_5 from viscous hydrodynamics with $\eta/s = 0.08$ for centralities 0-10% (upper left), 10-20% (upper right), 30-40% (lower left), and 40-50% (lower right). See Fig. 8 for 20-30% central collisions. Results are averaged over 100 events each. Experimental data from PHENIX [63].
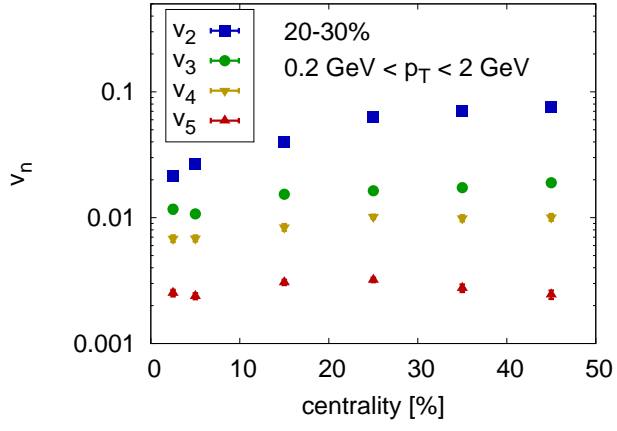
FIG. 14. (Color online) v_2 to v_5 as functions of centrality for $\eta/s = 0.08$. Averages are over 100 single events each.

[1] B. Schenke, S. Jeon, and C. Gale, Phys. Rev. **C82**, 014903 (2010).
[2] B. Schenke, (2011), arXiv:1106.6012 [nucl-th].
[3] R. Andrade *et al.*, Phys. Rev. Lett. **97**, 202302 (2006).
[4] A. Adare *et al.* (PHENIX), Phys. Rev. **C78**, 014901 (2008).
[5] B. I. Abelev *et al.* (STAR), Phys. Rev. Lett. **102**, 052302 (2009).
[6] B. Alver *et al.* (PHOBOS), Phys. Rev. **C81**, 024904 (2010).
[7] B. Alver *et al.* (PHOBOS), Phys. Rev. Lett. **104**, 062301 (2010).
[8] B. I. Abelev *et al.* (STAR), Phys. Rev. **C80**, 064912 (2009).
[9] M. Miller and R. Snellings, (2003), arXiv:nucl-ex/0312008.
[10] W. Broniowski *et al.*, Phys. Rev. **C76**, 054905 (2007).
[11] R. Andrade *et al.*, Phys. Rev. Lett. **101**, 112301 (2008).
[12] T. Hirano and Y. Nara, Nucl. Phys. **A830**, 191c (2009).
[13] J. Takahashi *et al.*, Phys. Rev. Lett. **103**, 242301 (2009).
[14] R. Andrade *et al.*, J. Phys. **G37**, 094043 (2010).
[15] B. Alver and G. Roland, Phys. Rev. **C81**, 054905 (2010).
[16] K. Werner, I. Karpenko, T. Pierog, M. Bleicher, and K. Mikhailov, Phys.Rev. **C82**, 044904 (2010).
[17] H. Holopainen, H. Niemi, and K. J. Eskola, Phys.Rev. **C83**, 034901 (2011).
[18] B. H. Alver, C. Gombeaud, M. Luzum, and J.-Y. Ollitrault, Phys.Rev. **C82**, 034913 (2010).
[19] H. Petersen, G.-Y. Qin, S. A. Bass, and B. Muller, Phys.Rev. **C82**, 041901 (2010).
[20] B. Schenke, S. Jeon, and C. Gale, Phys. Rev. Lett. **106**, 042301 (2011).
[21] B. Schenke, S. Jeon, and C. Gale, Phys. Lett. **B702**, 59 (2011).
[22] Z. Qiu and U. W. Heinz, Phys.Rev. **C84**, 024911 (2011).
[23] K. Dusling, Nucl.Phys. **A839**, 70 (2010), arXiv:0903.1764 [nucl-th].
[24] R. Chatterjee, H. Holopainen, T. Renk, and K. J. Eskola, Phys.Rev. **C83**, 054908 (2011), arXiv:1102.4706 [hep-ph].
[25] M. Dion, J.-F. Paquet, B. Schenke, C. Young, S. Jeon, and C. Gale, (2011), arXiv:1109.4405 [hep-ph].
[26] J. D. Bjorken, Phys. Rev. **D27**, 140 (1983).
[27] P. Huovinen, Quark Gluon Plasma 3 ed R C Hwa and X N Wang (Singapore: World Scientific) , 600 (2003), arXiv:nucl-th/0305064.
[28] P. F. Kolb and U. W. Heinz, Quark Gluon Plasma 3 ed R C Hwa and X N Wang (Singapore: World Scientific) , 634 (2003), arXiv:nucl-th/0305084.
[29] C. E. Aguiar, T. Kodama, T. Osada, and Y. Hama, J. Phys. **G27**, 75 (2001).

[30] T. Hirano, K. Morita, S. Muroya, and C. Nonaka, Phys. Rev. **C65**, 061902 (2002).
[31] T. Hirano, Phys. Rev. **C65**, 011901 (2002).
[32] T. Hirano and K. Tsuda, Phys. Rev. **C66**, 054905 (2002).
[33] C. Nonaka, E. Honda, and S. Muroya, Eur. Phys. J. **C17**, 663 (2000).
[34] C. Nonaka and S. A. Bass, Phys. Rev. **C75**, 014902 (2007).
[35] H. Niemi, G. S. Denicol, P. Huovinen, E. Molnar, and D. H. Rischke, Phys.Rev.Lett. **106**, 212302 (2011), arXiv:1101.2442 [nucl-th].
[36] H. Song, S. A. Bass, and U. Heinz, Phys.Rev. **C83**, 054912 (2011), arXiv:1103.2380 [nucl-th].
[37] W. A. Hiscock and L. Lindblom, Annals Phys. **151**, 466 (1983).
[38] W. A. Hiscock and L. Lindblom, Phys. Rev. **D31**, 725 (1985).
[39] S. Pu, T. Koide, and D. H. Rischke, Phys.Rev. **D81**, 114039 (2010).
[40] W. Israel, Ann. Phys. **100**, 310 (1976).
[41] J. Stewart, Proc.Roy.Soc.Lond. **A357**, 59 (1977).
[42] W. Israel and J. M. Stewart, Ann. Phys. **118**, 341 (1979).
[43] A. Muronga, Phys. Rev. Lett. **88**, 062302 (2002).
[44] R. Baier, P. Romatschke, D. T. Son, A. O. Starinets, and M. A. Stephanov, JHEP **04**, 100 (2008).
[45] A. Kurganov and E. Tadmor, Journal of Computational Physics **160**, 214 (2000).
[46] R. Naidoo and S. Baboolal, Future Gener. Comput. Syst. **20**, 465 (2004).
[47] H. Song and U. W. Heinz, Phys. Rev. **C77**, 064901 (2008).
[48] H. Song and U. W. Heinz, Phys. Rev. **C78**, 024902 (2008).
[49] M. D. Duez *et al.*, Phys. Rev. **D69**, 104030 (2004).
[50] B. Alver, M. Baker, C. Loizides, and P. Steinberg, (2008), arXiv:0805.4411 [nucl-ex].
[51] P. Jacobs, Eur. Phys. J. **C43**, 467 (2005).
[52] F. Wang (STAR), J. Phys. **G30**, S1299 (2004).
[53] J. Adams *et al.* (STAR), Phys. Rev. Lett. **95**, 152301 (2005).
[54] P. Huovinen and P. Petreczky, Nucl. Phys. **A837**, 26 (2010).
[55] K. Dusling, G. D. Moore, and D. Teaney, Phys. Rev. **C81**, 034907 (2010).
[56] A. M. Poskanzer and S. A. Voloshin, Phys. Rev. **C58**, 1671 (1998).
[57] R. Lacey, private communication (2011).
[58] R. S. Bhalerao and J.-Y. Ollitrault, Phys.Lett. **B641**, 260 (2006).
[59] S. S. Adler *et al.* (PHENIX), Phys. Rev. **C69**, 034909 (2004).

[60] B. B. Back *et al.*, Phys. Rev. Lett. **91**, 052303 (2003).

[61] P. Bozek, Phys. Rev. **C77**, 034911 (2008).

[62] A. Monnai and T. Hirano, Phys.Lett. **B703**, 583 (2011).

[63] A. Adare *et al.* (PHENIX Collaboration), (2011), arXiv:1105.3928 [nucl-ex].

[64] P. Huovinen, Eur.Phys.J. **A37**, 121 (2008), arXiv:0710.4379 [nucl-th].

[65] B. B. Back *et al.* (PHOBOS), Phys. Rev. **C72**, 051901 (2005).

[66] H.-J. Drescher and Y. Nara, Phys.Rev. **C76**, 041903 (2007).